

Structural and Energetic Landscape of Fluorinated 1,4-Phenylenediboronic Acids

Published as part of the *Crystal Growth & Design* virtual special issue In Honor of Prof. G. R. Desiraju

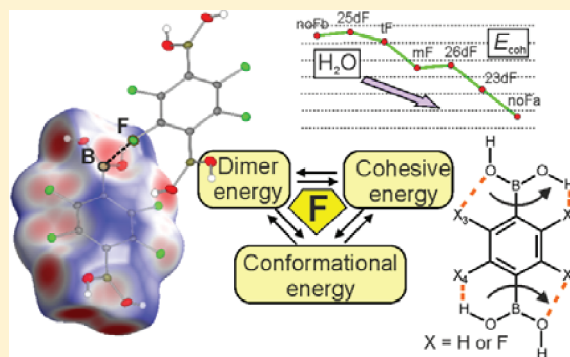
Krzysztof Durka,^{*,‡,§} Katarzyna N. Jarzemska,^{†,§} Radosław Kamiński,[†] Sergiusz Luliński,[‡] Janusz Serwatowski,[‡] and Krzysztof Woźniak^{*,†}

[†]Department of Chemistry, University of Warsaw, Pasteura 1, 02-093, Warszawa, Poland

[‡]Department of Chemistry, Warsaw University of Technology, Noakowskiego 3, 00-664, Warszawa, Poland

S Supporting Information

ABSTRACT: The results of X-ray crystallographic and computational studies of a series of fluorinated 1,4-phenylenediboronic acids (i.e., fluoro-1,4-phenylenediboronic acid, 2,6-difluoro-1,4-phenylenediboronic acid, 2,3-difluoro-1,4-phenylenediboronic acid, 2,5-difluoro-1,4-phenylenediboronic acid, and tetrafluoro-1,4-phenylenediboronic acid) are reported. The effect of fluorine substitution on crystal organization in the presence of strong and directional hydrogen bonds was studied. Comparison with the two previously reported forms of the unsubstituted 1,4-phenylenediboronic acid revealed a strong relation between a supramolecular network and the number of water molecules present in the crystal lattice. As indicated by the theoretical calculations performed in the CRYSTAL and PIXEL programs, the structures with greater amount of water are better stabilized (from about $-170 \text{ kJ}\cdot\text{mol}^{-1}$ for anhydrous forms to about $-420 \text{ kJ}\cdot\text{mol}^{-1}$ for tetrahydrate). The energy of hydrogen bonded dimers vary from $-40 \text{ kJ}\cdot\text{mol}^{-1}$ to $-50 \text{ kJ}\cdot\text{mol}^{-1}$. Contacts with fluorine atoms play rather a secondary role in the crystal packing. Fluorine substituents tend to interact with the electropositive boron atom. Furthermore, intramolecular interactions significantly affect the torsion angle of the $\text{B}(\text{OH})_2$ group. The constrained energy scan revealed that stronger interactions with substituents stabilize the planar conformation and hamper the rotation of the boronic group. This in turn has a further impact on the interactions within selected crystal motifs and supposedly rules the proton disorder within boronic fragments. Besides the interactions with the fluorine atoms, other weak contacts such as $\text{C}(\pi)\cdots\text{B}$ and $\text{O}\cdots\text{B}$ also influence the molecular organization. The energy of the corresponding dimers varies from $-15 \text{ kJ}\cdot\text{mol}^{-1}$ to $-25 \text{ kJ}\cdot\text{mol}^{-1}$.



1. INTRODUCTION

The understanding of molecular organization in the solid state enables researchers to control supramolecular entity formation and to produce crystal networks with desired structural features and properties. Strong and directional hydrogen bonds, and many diverse self-complementary hydrogen-bonding groups (e.g., amide or carboxylic groups), are commonly used for the purpose of such strategies.¹ Recent reports focus on using the $\text{B}(\text{OH})_2$ unit of boronic acids as a building block in the formation of hydrogen-bonded structures.² Although boronic acids are not as commonly studied as carboxylic acids and amides, numerous applications of these compounds have been reported.³ For instance, the Suzuki cross-coupling reaction is one of the most popular methods for carbon–carbon bond formation.⁴ Boronic acids are also widely used in medicine, for example, in antitumor treatment,⁵ whereas in material science they act as nonlinear optical chromophores.⁶ More recently, boron compounds have been applied in condensation reactions with polyols to create new functional materials such as macrocycles,

cages, polymers, and porous covalent organic frameworks (COFs).⁷

Among the determined crystal structures of various boronic acids, a great majority forms a dimeric motif of $\text{B}(\text{OH})_2$ moieties (also being characteristic for carboxylic acids and amides).^{2a–m} Introduction of the second boronic group offers a higher level of self-assembly by extending the hydrogen-bonded structure in new directions. Surprisingly, despite some striking examples found in the literature, diboronic acids have not been well explored in the context of supramolecular network formation to date. Up to now, the Cambridge Structural Database (CSD)⁸ contains only a few structures of diboronic acids.^{2h–m}

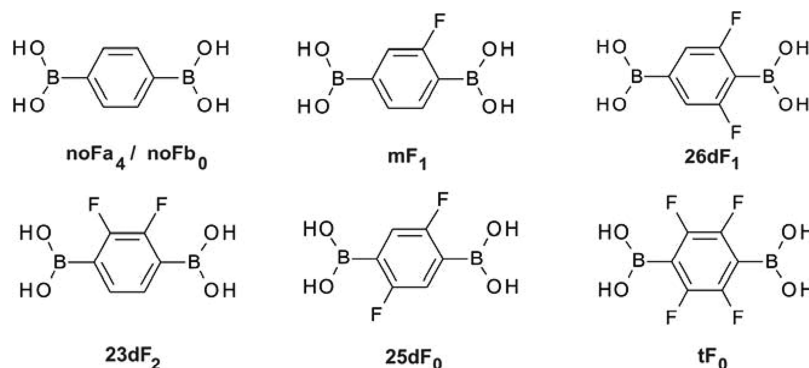
Apart from relatively strong hydrogen bonds, as these present in the structures of boronic and diboronic acids, also weaker interactions, for example involving the fluorine atom, are of current interest in modern supramolecular chemistry.⁹

Received: April 17, 2012

Revised: May 15, 2012

Published: May 21, 2012

Scheme 1. Studied 1,4-Phenylenediboronic Acid Derivatives: 1,4-Phenylenediboronic Acid (noFa_4 – tetrahydrate;²¹ noFb_0 – anhydrous form^{2m}), Fluoro-1,4-phenylenediboronic Acid (mF_1), 2,6-Difluoro-1,4-phenylenediboronic acid (26dF_1), 2,3-Difluoro-1,4-phenylenediboronic Acid (23dF_2), 2,5-Difluoro-1,4-phenylenediboronic Acid (25dF_0), and Tetrafluoro-1,4-phenylenediboronic Acid (tF_0)^a



^aThe subscript provides information about the water content.

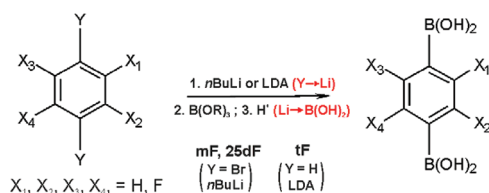
According to recent reports, the replacement of hydrogen by fluorine atoms may lead to some distinct changes in-between initial and resulting crystal structures¹⁰ and then is reflected in the reactivity¹¹ and biological activity of the analyzed compounds.¹² A number of studies have been carried out to establish the role of fluorine atom in crystal engineering, especially in generating different packing motifs via weak $\text{X}\cdots\text{H}\cdots\text{F}$ ($\text{X} = \text{O}, \text{N}, \text{C}$), $\text{F}\cdots\text{F}$, or $\text{F}\cdots\pi$ interactions.^{10,11} Nevertheless, the nature of these contacts still remains a matter of discussion.

In this paper we focus our attention on a series of fluorinated 1,4-phenylenediboronic acid derivatives (Scheme 1). We discuss their molecular and supramolecular structures, the role of the water molecules, and the fluorine atom substitution effect, by comparing the obtained structures with the two previously reported pseudopolymorphs of 1,4-phenylenediboronic acid: tetrahydrate (noFa_4)²¹ and anhydrous (noFb_0)^{2m} forms. The redistribution of electron density caused by the fluorine substituent is crucial for weak intermolecular interactions. It influences the geometrical arrangement of boron and oxygen atoms, and affects the electronic structure of aromatic rings. Thus, our study is devoted to understanding of binding properties and the specificity of intermolecular contacts present in the investigated systems. For this purpose the X-ray structural analysis was performed and supplemented by a comprehensive computational characterization.

2. MATERIALS AND METHODS

2.1. Synthesis. Diboronic acids 26dF and 23dF were synthesized in accordance with the procedure already published in the literature.¹³ In turn, the syntheses of mF and 25dF were accomplished using a double step-by-step lithiation/boronation procedure applied to the respective bromofluorobenzenes, followed by hydrolysis of the obtained derivatives (Scheme 2). The synthesis of tF was less

Scheme 2. General Synthetic Scheme of Fluorinated 1,4-Phenylenediboronic Acids



straightforward, which is because highly reactive lithium intermediates are very susceptible to degradation. After numerous attempts, tF was finally synthesized by employing a double in situ lithiation/boronation of a 1,2,4,5-tetrafluorobenzene, using lithium diisopropylamide (LDA) as lithiating and $\text{B}(\text{O}i\text{Pr})_3$ as boronating agents, respectively. Single-crystals, suitable for X-ray diffraction experiments, were obtained by crystallization from various solvent mixtures containing toluene, acetone, and water. It is worth noting that, although the trifluoro derivative ($\text{C}_6\text{H}_3\text{BF}_3\text{O}_4$) was synthesized, all attempts of crystal growing were unsuccessful. More detailed information about synthetic and crystallization procedures is available in the Experimental Section and Supporting Information.

2.2. Geometries and Energy Computations. Careful structure determination and preparation were found to be crucial for further energy analysis and drawing conclusions. Therefore, here we present the main information regarding methods and proceedings. Full details of the X-ray diffraction data collection, crystal structure determination, and theoretical methods are located in the Experimental Section and Supporting Information.

For the purpose of the molecular and supramolecular structure analysis and energy computation, all $\text{X}\cdots\text{H}$ bond distances ($\text{X} = \text{non-hydrogen atom}$) were set to the average neutron values.¹⁴ Additionally, geometry optimization in the *CRYSTAL09*¹⁵ program was performed to derive more appropriate hydrogen atom positions, that is, not only $\text{X}\cdots\text{H}$ bond length but also its direction (see Experimental Section). Such an approach is crucial for a proper description of interactions involving hydrogen atoms and thus has a significant impact on lattice and dimer interaction energy estimation. For instance, the computational study of two isomorphs, mF_1 and 26dF_1 , based on the X-ray geometries with $\text{X}\cdots\text{H}$ bonds simply extended to neutron-normalized distances, showed a significant cohesive energy difference, which amounted to over $50 \text{ kJ}\cdot\text{mol}^{-1}$ for the benefit of mF_1 (Table 2). The differences between the experimental and optimized crystal structure of 26dF_1 were especially noticeable for the hydrogen atom positions (Figure 4S in the Supporting Information). The subsequent cohesive energy calculation and dimer interaction energy estimations gave values much closer to the results obtained for its isostructural diboronic acid derivative, mF_1 , as previously expected.

Computational analysis also helped to detect a certain structural inadequacy in the case of noFa_4 . Careful study of the literature-reported noFa_4 structure revealed that one of the water molecules (indicated by the O5 oxygen atom in the CSD file) was incorrectly oriented. As a consequence, the two symmetry equivalent hydrogen atoms were found pointing toward each other, being at a very short distance of about 1.14 \AA . This causes some destabilization and influences the total cohesive energy value. To find a proper arrangement, the full periodic geometry optimization was performed. The obtained cohesive energy value for the optimized crystal structure

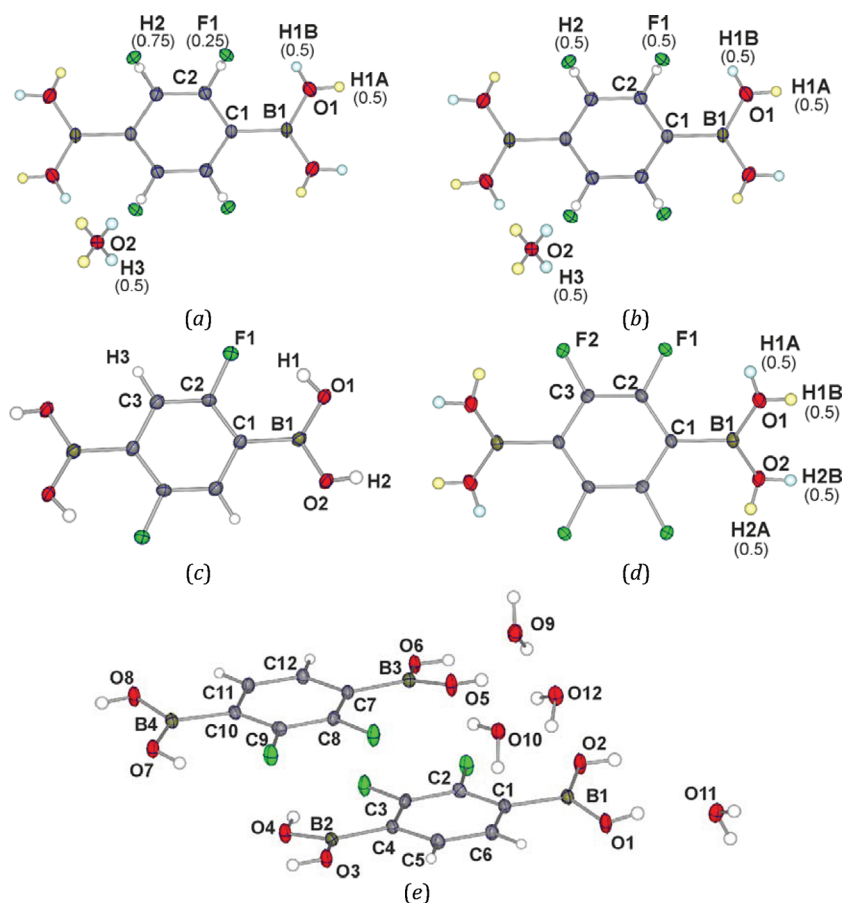


Figure 1. Labeling of atoms and the atomic thermal motion estimation as ADPs (50% probability level) for (a) **mF₁**, (b) **26dF₁**, (c) **25dF₀**, (d) **tF₀**, and (e) **23dF₂**. Site occupancy factors of disordered atoms are given in parentheses. Disordered hydrogen atoms are marked in different colors.

is 36 kJ·mol^{−1} lower (which corresponds to the energy of a medium strength hydrogen bond) than that calculated for the reported **noFa₄** structure, with the X–H bond lengths set to the average neutron distances.

The above-mentioned examples show that not only the X–H bond lengths, but also their directionality are crucial for a proper hydrogen bond description, and thus subsequent structural and energetic studies.¹⁶ Averaged neutron-derived X–H bond distances are related to the optimized geometries and thus are reported without estimated standard deviations. In order to validate the *CRYSTAL* results, we have also evaluated cohesive energies by the means of the *PIXEL* approximation (see Experimental Section).¹⁷ *PIXEL* and *CRYSTAL* energy values were found to be consistent. Additionally, the *PIXEL* program allows for estimating the total energy components, which gives an extra insight into the nature of interactions.

The presence of the fluorine substituent has a significant impact on the structure stabilization and interaction energies within the selected supramolecular motifs. Hence, in the first part of the discussion, we compare the molecular geometries of the studied compounds, and afterward, we systematically analyze their supramolecular structures. Among the analyzed systems, four basic groups, characterized by a different amount of solvent incorporated into the crystal lattice, can be distinguished. These are waterless structures formed by **noFb₀**, **25dF₀**, and **tF₀**, then networks containing one (**26dF₁** and **mF₁**), two (**23dF₂**), and four (**noFa₄**) water molecules per one molecule of the diboronic acid. To approach this complex problem, we present and

compare crystal structures and related computational results for the compounds belonging to each of the previously defined classes. Subsequently, we confront all the classes and discuss their energetic landscape in a wider context.

3. RESULTS AND DISCUSSION

3.1. Molecular Structure Description. Generally, different fluorine substitutions only slightly influence bond lengths between non-hydrogen atoms. The largest deviations are found for the B–C, B–O, and C–F bonds. Geometrical parameters and the corresponding plots are given in Table 1S in the Supporting Information, whereas the molecular geometries are illustrated in Figure 1. Nevertheless, while switching from the unsubstituted to the tetrafluoro-substituted derivative, no structural trend regarding B–O distances, reflecting a fluorine atom influence, becomes obvious. In the case of the B–C bond, its length slightly increases, when hydrogen atoms are replaced by fluorine atoms, but again the correlation is not clear. Solely the presence of four fluorine atoms at the phenyl ring gives a significant B–C bond elongation, and, consequently, the B–O bond shortening. It is, however, important to note that B–O distances are in general much shorter (by about 0.03 Å) in a crystal lattice than in the corresponding optimized isolated molecules. This is obviously caused by the hydrogen bond pattern formation (i.e., in general crystal field effects). Similarly, in the case of the C–F distances, no visible trend is observed. The X-ray-determined **mF₁** and **26dF₁** diboronic acid structures exhibit the shortest C–F bonds (ca. 1.33 Å), which is, however, caused by the presence of disorder. This is in contrast

to the optimized crystal lattices, where the C–F distances are comparable among all the studied derivatives (see Supporting Information).

As indicated by the C2–C1–B1–O1 dihedral angle (hereafter abbreviated as τ), the boronic groups in **noFb₀**, **mF₁**, **26dF₁**, **25dF₀**, and **tF₀** are significantly rotated along the carbon–boron bonds by about 18.8–37.6°. In the **23dF₂** and **noFa₄** structures they remain almost planar, regarding the aromatic ring planes. High flexibility of the B(OH)₂ group is also characteristic for other structures of boronic acids and their derivatives. The CSD search gives the whole spectrum of τ angles, starting from planar conformations ($\tau = 0^\circ$) and ending with perpendicular ones ($\tau = 90^\circ$) for *ortho*-sterically hindered boronic acids (Figure 3S in the Supporting Information). In order to support the discussion with the energy landscape for *para*-diboronic acids, we have performed a series of computations for three model compounds: phenylboronic acid (**phba**) and its 2-fluoro (**2Fphba**) and 2,6-difluoro (**26dFphba**) derivatives. The results of τ -constrained optimization (the τ angle varies from 0° to 90° in steps of 5°, performed at the MP2¹⁸/aug-cc-pVTZ¹⁹ level of theory) revealed that the planar conformation is the most stable one (Figure 2). It is a well-known phenomenon that the rotation of

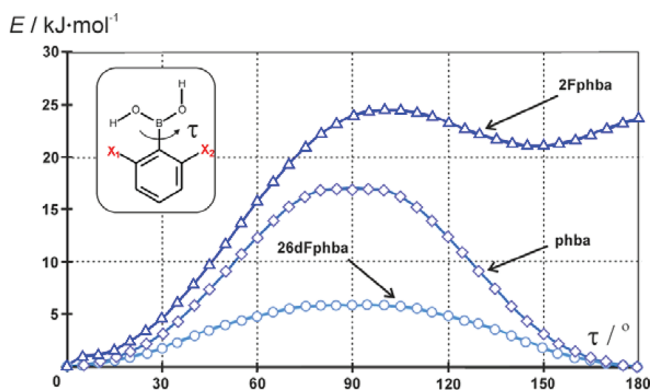


Figure 2. τ -Constrained optimization performed at the MP2/aug-cc-pVTZ level of theory. Numerical values are deposited in Table S5 in the Supporting Information.

the B(OH)₂ group leads to a decreased charge transfer from the aromatic ring to the boron atom. Apart from the conjugation effects, the intramolecular contacts with the hydrogen or fluorine atoms located in the *ortho* position(s) significantly influence the relative molecular stabilization energy. It was then possible to estimate the energy values of individual intramolecular contacts on the basis of the comparative computations prepared for all model compounds with the B(OH)₂ group in *syn-syn*, *syn-anti*, or *anti-anti* conformations (Table 1). Contributions from the two hydroxyl groups, together with the conjugation effect, sum up closely to rotation barriers of the B(OH)₂ group and indicate a relative conformational stability of the compound. For instance, the weak intramolecular C–H...O interactions between the oxygen atom from the *syn*-conformed hydroxyl group and the *ortho*-positioned hydrogen atom stabilize the planar conformation and therefore increase the rotation barrier in **phba**. This effect is partially counterbalanced by the repulsion between the hydrogen atom from the second *anti*-conformed hydroxyl group and the hydrogen atom from the *ortho* position at the aromatic ring. In **2Fphba**, one of the repulsive C–H...H–O contacts is replaced by the

Table 1. Estimated Energy Values of Selected Intramolecular Contacts (E_i)^a

atom	conformation			
	syn		anti	
	contact	$E_i/\text{kJ}\cdot\text{mol}^{-1}$	contact	$E_i/\text{kJ}\cdot\text{mol}^{-1}$
H	C–H...O	–13	C–H...H–O	3
F	C–F...O	4	C–F...H–O	–3

^aDetails are available from the Supporting Information.

intramolecular C–F...H–O interaction. This increases the stability of planar conformation and increases the rotation barrier by ca. 7 kJ·mol^{–1}. On the other hand, in the **26dFphba** model molecule, the repulsion between the fluorine atom and the oxygen atom from the *syn*-conformed OH group facilitates the rotation. The conjugation of boron atom with the aromatic ring amounts to about 6 kJ·mol^{–1} and depends on the number of fluorine substituents. In the case of the derivatives richer in fluorine atoms, the charge transfer from aromatic ring to the boron atom is less pronounced. For example, for the tetrafluorinated phenylboronic acid the conjugation energy is equal to ca. 4.5 kJ·mol^{–1}.

The molecular flexibility features of the model **2Fphba** and **26dFphba** molecules can be directly related to the fluorinated diboronic acids. The structures of **25dF₀**, **23dF₂**, and **mF₁** resemble **2Fphba**, while **tF₀** and **26dF₁** resemble **26dFphba**. Isolated molecule computation results show that the planar conformation is the most stable one. However, at the lower τ -angle range, the rotation energy requirement for the boronic acid group is relatively small (rotation from $\tau = 0^\circ$ to $\tau = 30^\circ$ requires 2 – 5 kJ·mol^{–1} for one boronic group). Therefore, in the presence of crystal field, boronic groups deviate from the planarity and the magnitude of such a deviation clearly depends on the number and positions of fluorine substituents.

Intramolecular contacts have also a visible influence on the atomic angles around the boron atom. Because of the existence of the C–H...O interaction, the C–B–O angles reach quite small values of about 116°. In the presence of the repulsive C–H...H–O contacts, they are larger than 120°. Similarly, the C–F...H–O interaction formation leads to the increased C–B–O angle (123–125°). Despite the repulsive nature of the C–F...O interaction, the *syn*-conformed hydroxyl group gains more flexibility and the angle is fairly close to 119°. The obtained data are given in Table 1S in the Supporting Information, while the geometrical deviations are summarized in Figure 2S.

3.2. Supramolecular Structures of noFb₀, 25dF₀ and tF₀. The **25dF₀** and **tF₀** compounds crystallize in the triclinic *P* $\bar{1}$ and monoclinic *P*2₁/*n* space groups, respectively. Molecules in both crystal structures are closely packed, with no solvent content. We found that **25dF₀** is structurally isomorphic to the previously reported **noFb₀** (Figure 4). In the case of the **tF₀** compound, the residual density maps reveal hydrogen atom disorder in the B(OH)₂ fragments, whereas in the **25dF₀** structure all atom positions are ordered (Figure 1S in the Supporting Information). In the latter case the diboronic acid moieties adopt a well-defined *syn-anti* conformation.

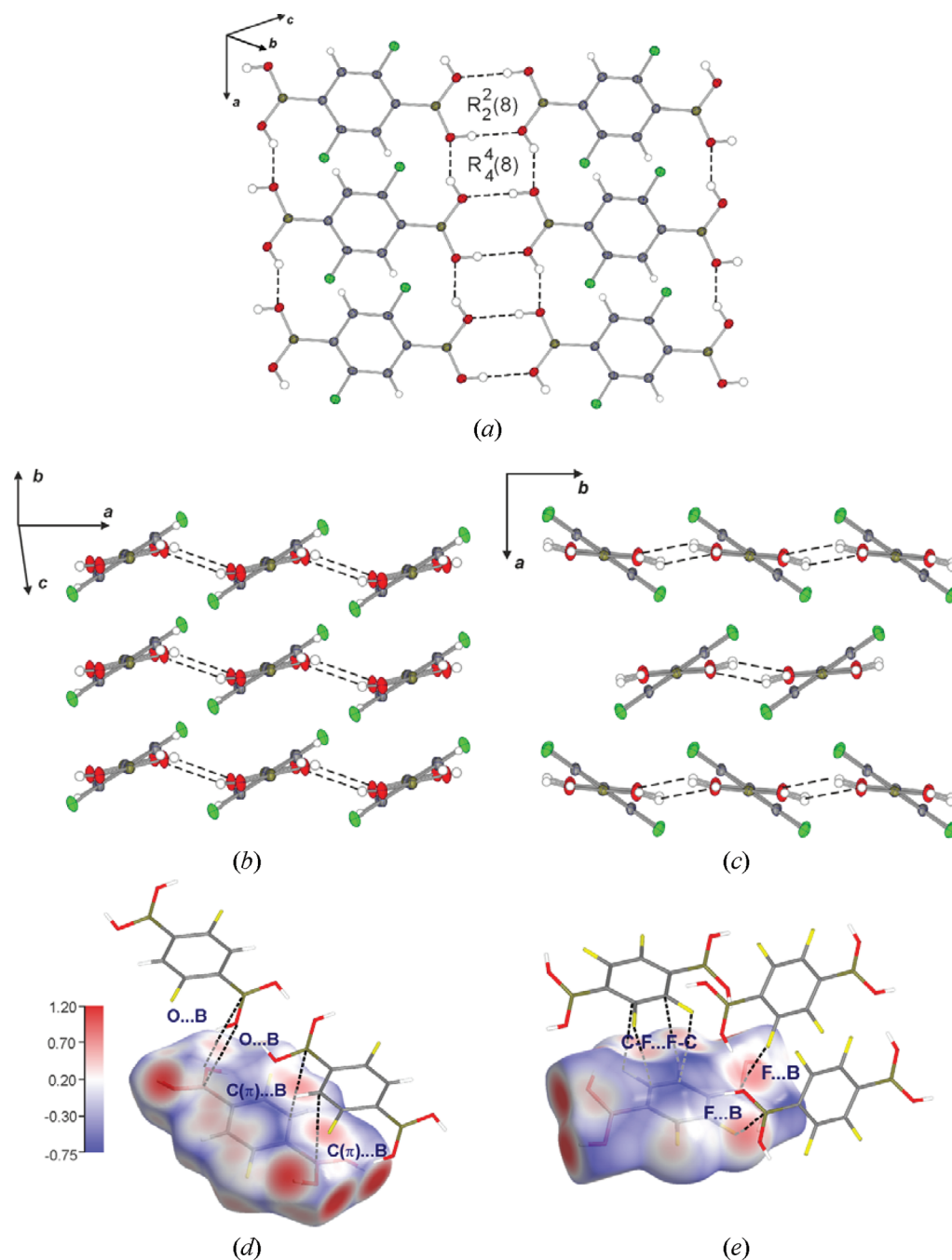


Figure 3. (a) Molecular layers and their further aggregation in **25dF₀** (b) and **tF₀** (c). Hirshfeld surfaces for the **25dF₀** (d) and **tF₀** (e) molecules, with a d_{norm} property mapped in the range from -0.75 to 1.20 (selected neighboring molecules and weak interactions are shown).

Similar to **noFb₀**, the **25dF₀** and **tF₀** molecules form hydrogen-bonded sheets parallel to the (01 $\bar{1}$) and (100) crystal planes, respectively. Diboronic acid moieties are linked via centrosymmetric R₂²(8) and R₄⁴(8) units within the two-dimensional (2D) molecular motifs (Figure 3a). Nevertheless, **25dF₀** and **noFb₀** exhibit quite a different picture of the supramolecular layered assembly with respect to **tF₀**. The molecules of both **noFb₀** and **25dF₀** are held together by weak dimeric C(π)⋯B and O⋯B interactions, which leads to the parallel orientation of the molecules from adjacent layers (Figure 3b). These contacts are very visible as bright red spots (i.e., close-range contacts) on the corresponding Hirshfeld surface²⁰ (Figure 3d). In turn, the layered aggregation in the case of **tF₀** is based on the F⋯B

interactions as indicated by the flat red regions on the Hirshfeld surface (Figure 3e). The above-mentioned F⋯B contacts are also reflected in the 2D fingerprint plot as the increased concentration of points located in the upper part of the two characteristic spikes (Figure 4). Additionally, there are bright red spots on the Hirshfeld surface near the C–F bond. It seems that this corresponds to the interaction between the two antiparallel C–F groups (the distance amounts to 2.955 Å). However, the small C–F⋯F angle value (79.0°) suggests that this is not a typical F⋯F interaction. This contact may also result from the packing of molecules in the crystal lattice. In contrast to the structures of **noFb₀** and **25dF₀**, the crystal planes derived from the aromatic rings from the adjacent layers

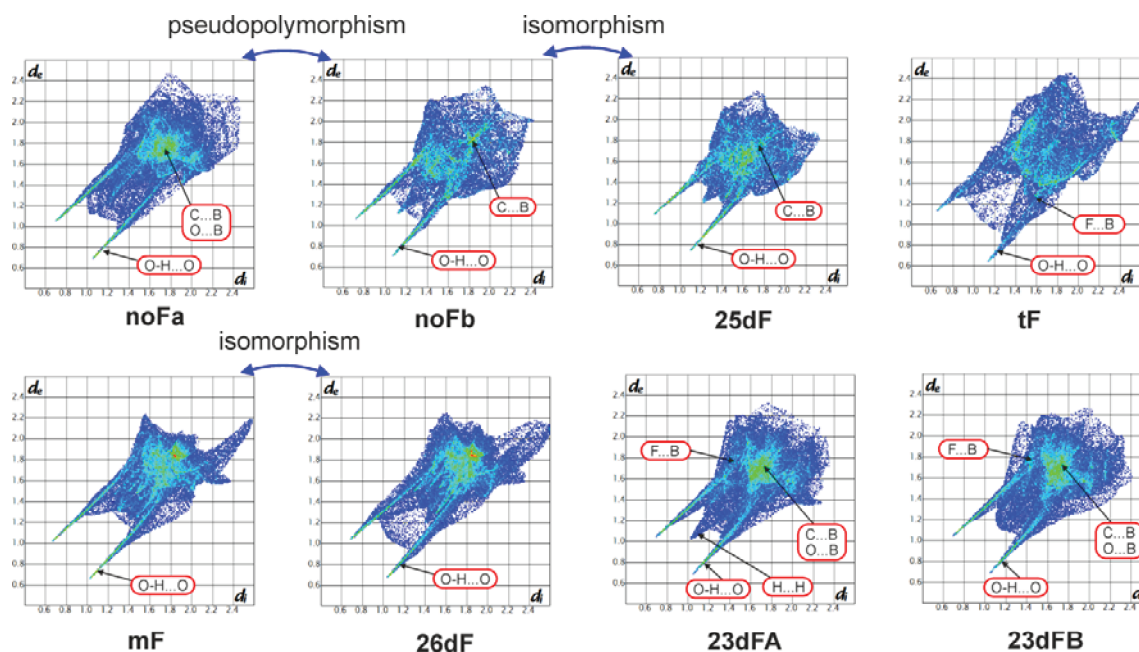


Figure 4. Fingerprint plots of the Hirshfeld surfaces for each independent molecule in the structures of 1,4-phenylenediboronic acids (fingerprint plots are based on the X-ray geometries; the most important intermolecular contacts are marked; more intense colors represent a more dense accumulation of points).

Table 2. Cohesive Energy Values Calculated for the Molecules with the Geometry Taken from the Crystal Structures after All X–H Bonds Set to Standardized Neutron Values ($E_{\text{coh}}^{\text{X-ray}}$), and for the Optimized Geometries ($E_{\text{coh}}^{\text{opt}}$)^a

Compound	CRYSTAL		PIXEL
	$E_{\text{coh}}^{\text{X-ray}}$ / kJ·mol ^{−1}	$E_{\text{coh}}^{\text{opt}}$ / kJ·mol ^{−1}	$E_{\text{coh}}^{\text{opt}}$ / kJ·mol ^{−1}
noFb ₀	−168.9	−177.6	−179.4
25dF ₀	−162.0	−168.3	−168.3
tF ₀	−186.0	−195.2	−181.6
mF ₁	−271.0	−273.2	−273.8
26dF ₁	−219.5	−266.5	−258.8
23dF ₂	−313.0	−342.4	
noFa ₄	−384.5	−420.4	

^aThe calculations were carried out with the CRYSTAL and PIXEL programs.

in tF₀, fitted by the least-squares method, are not parallel (Figure 3c). The interplanar angle is equal to 70.6°. Furthermore, the C(π)⋯B interactions, characteristic for noFb₀ and 25dF₀, were not observed in the case of the tF₀ structure.

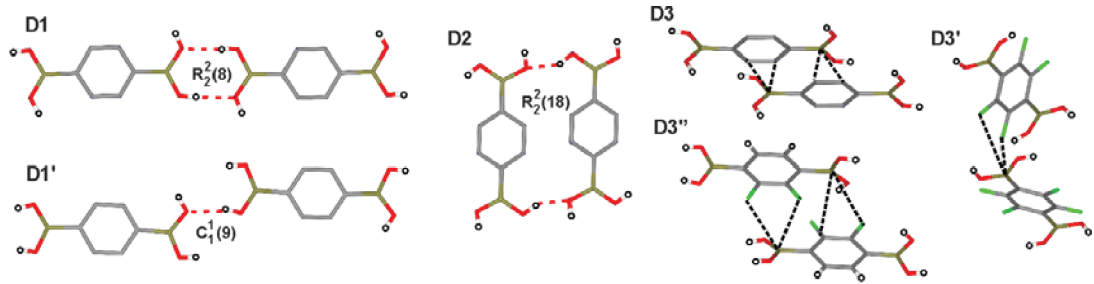
Periodic computations carried out with the CRYSTAL and PIXEL programs (Table 2) confirm the structural resemblance of noFb₀ and 25dF₀. The cohesive energy value differs significantly for tF₀, being about 20 kJ·mol^{−1} lower than in the case of noFb₀ and 25dF₀. Tetrafluorodiboronic acid is more compact in packing, which is reflected in its overall more advantageous stabilization energy. 25dF₀ was found to be least stabilized among compounds belonging to this group.

Two types of diboronic acid dimers characterized by the lowest interaction energies can be distinguished in each of the three analyzed structures (Table 3). These are hydrogen bonded dimers creating molecular chains via boronic acid groups (D1 – motif R₂²(8)), and boronic acid dimers

connecting two neighboring chains together (D2 – motif R₂²(16)). The pattern is shown in Figure 3c, whereas the particular dimers are presented in Table 3. The distance between aromatic ring centroids in D1 dimers is the same for 25dF₀ and tF₀ (10.167 Å) and a little bit shorter for noFb₀ (10.095 Å). However, as indicated by the O⋯O distances (2.733 Å, 2.789 Å and 2.735 Å for noFb₀, 25dF₀, and tF₀, respectively), the hydrogen bond length is the shortest in the case of tF₀. Such a shortening of hydrogen bonds in tF₀ is counterbalanced by the significant stretching of molecules along the Z direction. Despite some differences in the geometries of hydrogen bonds, the D1 dimer interaction energies seem to be quite alike among these three compounds.

A different situation is observed for the D2 dimers, where the O⋯O distance correlates with the torsion angle of the B(OH)₂ group along the B–C bond. A significant value of τ in the case of tF₀ (30.5°) guarantees stronger hydrogen interactions within

Table 3. Schematic Representations of Fluorinated Diboronic Acid Dimers Together with the Interaction Energies (E_D) Calculated with CRYSTAL at the DFT(B3LYP)/6-31G(d,p) Level of Theory and the Corresponding Geometrical Parameters^a



compound	dimer	$E_D/\text{kJ}\cdot\text{mol}^{-1}$	interaction	$d_{X\cdots A}$ (Å)	d_{D-X} (Å)	$d_{D\cdots A}$ (Å)	$\theta_{D-X\cdots A}$ (°)
noFb₀	D1	−47.3	O1–H1 \cdots O2 ^{#1}	1.733	0.987	2.719	176.8
	D2	−56.1	O2–H2 \cdots O1 ^{#2}	1.825	0.980	2.734	152.7
	D3	−15.5	C2 \cdots B1 ^{#3} C3A \cdots B1 ^{#3}	3.762 3.510			
25dF₀	D1	−49.6	O1–H1 \cdots O2 ^{#1}	1.789	0.984	2.770	174.6
	D2	−44.2	O2–H2 \cdots O1 ^{#2}	2.003	0.975	2.858	145.3
	D3	−18.5	C2 \cdots B1 ^{#3} C3 \cdots B1 ^{#3}	3.562 3.295			
tF₀	D1	−45.3	O1–H1A \cdots O2 ^{#4}	1.735	0.987	2.721	175.6
	D2	−68.1	O2–H2A \cdots O1 ^{#4}	1.841	0.979	2.712	156.7
	D3'	−13.8	F1 \cdots B1 ^{#5} F2 \cdots B1 ^{#5}	3.445 2.930			
mF₁	D1	−43.8	O1–H1B \cdots O1 ^{#6}	1.668	0.990	2.658	178.0
26dF₁	D1	−43.1	O1–H1B \cdots O1 ^{#6}	1.690	0.989	2.679	179.2
23dF₂	D1'	−23.4	O2–H2 \cdots O7 ^{#7}	1.691	0.987	2.673	172.6
	D3''	−25.0	C5 \cdots B4 ^{#8}	3.406			
			C6 \cdots B4 ^{#8}	3.213			
			F3 \cdots B2 ^b	3.132			
			F4 \cdots B2 ^b	3.525			
			C8 \cdots B1 ^{#8}	3.424			
			C9 \cdots B1 ^{#8}	3.226			
noFa₄	D3	−20.9	F1 \cdots B3 ^b	3.178			
			F2 \cdots B3 ^b	3.516			
			O2–H2 \cdots O1 ^{#9}	1.752	0.983	2.726	170.2
			C2 \cdots B1 ^{#10}	3.388			
			C3 \cdots B1 ^{#10}	3.225			
			C5 \cdots B2 ^{#10}	3.401			
			C6 \cdots B2 ^{#10}	3.228			

^a d and θ denote distance and angle, respectively. ^bStands for intramolecular contact. Symmetry transformations: (#1) $x + 1, y, z$; (#2) $-x, -y - 1, -z + 1$; (#3) $x, y + 1, z$; (#4) $-x + 1, -y + 1, -z + 1$; (#5) $-x - 1.5, y + 0.5, -z - 0.5$; (#6) $x, y, -z + 1$; (#7) $x - 1, y, z + 1$; (#8) $x - 1, y, z$; (#9) $-x + 3, -y + 1, -z + 1$; (#10) $x - 1, y, z$.

the **D2** dimers (the O \cdots O of 2.712 Å), and thus much more efficient packing. For **noFb₀**, the deviation of the B(OH)₂ group from the aromatic ring planarity is less pronounced (26.2°) and the O \cdots O distance is equal to 2.734 Å, whereas for **25dF₀** the C2–C1–B1–O1 torsion angle amounts to 20.4° and the O \cdots O distance to 2.858 Å. Both the angle and distance values correlate perfectly with the **D2** stabilization energy magnitudes. In the case of **tF₀**, the **D2** dimer is the most, while for **25dF₀** the least stabilized one. It is also interesting to note that in the structures of **noFb₀** and **tF₀**, the **D2** dimers were found to be better stabilized than these of the **D1** type.

As mentioned before, all three structures form well-defined molecular layers via the discussed motifs (Figure 3b,c). Therefore, in order to analyze the impact of dispersive interactions on the crystal architecture stability, the interlayer stabilization energies were evaluated. It comes out that the energy values are comparable between **25dF₀** and **tF₀**, being equal to −61.6 kJ·mol^{−1} and

−57.8 kJ·mol^{−1}, respectively. They are though slightly less beneficial in the case of **noFb₀** (−50.4 kJ·mol^{−1}). Nevertheless, the energetic results do not resemble the interlayer distance sequence, which is 3.702 Å for **noFb₀**, 3.787 Å for **25dF₀**, and 4.315 Å for **tF₀**. Such an outcome is caused by a number of competitive factors, that is, the character of the neighboring layers, the presence of fluorine atoms influencing the atom net charges, and then the interlayer distances. Even though the interlayer distance is shortest in the case of **noFb₀**, the layer pattern is clearly less stabilized than in **25dF₀**. This is due to the better stabilized **D3** dimer type and the smaller B(OH)₂ group torsion angle value, which enables the intensified intermolecular contacts. Furthermore, in the case of **tF₀**, molecular layers, being more distant, are differently mutually arranged than in **noFb₀** and **25dF₀**. Therefore, the interaction energy is less advantageous than for **25dF₀**.

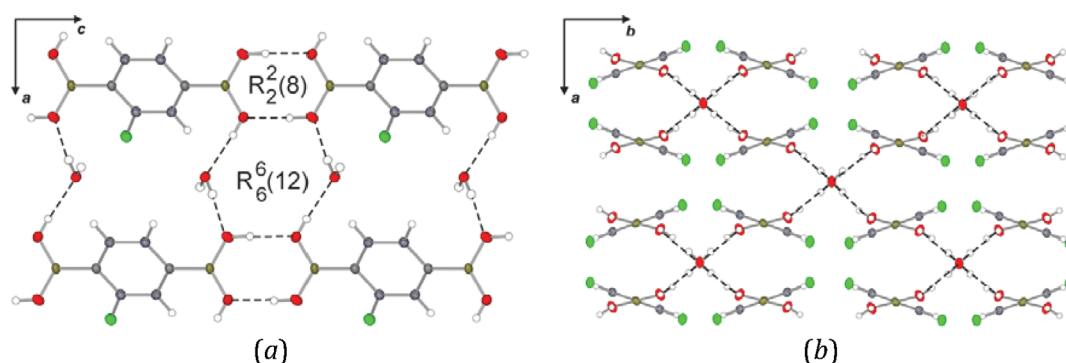


Figure 5. Hydrogen-bonded chains of diboronic acids and their arrangement with the water molecules within **mF₁** and **26dF₁** (only one occupied site is presented for clarity) (a) 2D layers and (b) 3D catenated network.

3.3. Supramolecular Structure of **mF₁ and **26dF₁**.** The **mF₁** and **26dF₁** acids are isostructural and both crystallize as monohydrates in the orthorhombic *Cccm* space group. As a consequence of the statistical disorder, the molecules occupy a special position at the inversion center and a mirror plane. The refinement shows that each of the four sites is occupied by 0.25:0.75 and 0.5:0.5 ratio of fluorine to hydrogen atoms for the structures of **mF₁** and **26dF₁**, respectively. Similarly, the hydrogen atoms belonging to the B(OH)₂ groups and water molecules can occupy two sites. Because of the presence of the disorder, and because of the fact that in the asymmetric part of the unit cell there is a half of the molecule, detailed analysis of the intermolecular interaction patterns using the standard Hirshfeld surface methods and *CRYSTAL* computations is hampered. Therefore, for the purpose of the further analysis, we have lowered the symmetry of the system from the *Cccm* space group to the *P2₁/n* one (metric properties were unchanged), preserving geometrical parameters and removing the disorder. The presence of the disorder allows a few combinations of the fluorine derivative mutual arrangement in the crystal lattice. However, computational study of these different possibilities revealed that there is almost no energy difference among them (Table 6S in the Supporting Information). Consequently, to simplify the problem, we chose a certain molecular arrangement for **mF₁** and **26dF₁** to remove the disorder, as illustrated in Figure 5a.

According to expectations, every molecule of diboronic acid interacts with its two neighbors in the centrosymmetric R₂²(8) synthon, leading to a hydrogen-bonded chain formation along the *Z* direction (Figure 5a, motif R₂²(8)). The O...O distance for **mF₁** compound is equal to 2.658 Å (Table 3), while for **26dF₁** it is a little bit longer and amounts to 2.679 Å. The D1 dimer energies are comparable in both cases. Water molecules built into the crystal lattice act as two donors and two acceptors of hydrogen bonds formed with the boronic groups. Therefore, they link four neighboring diboronic chains into a three-dimensional (3D) catenated network (Figure 5a, motif R₆⁶(12)). Water molecules, being less acidic than diboronic acid species, interact more efficiently as boronic acid proton acceptors rather than donors. This is a consequence of the weakened basicity of the oxygen atoms belonging to the boronic fragment, donating electrons toward the *p* orbitals of the boron atom. The interaction energy values, between the water and the boronic acid, obtained for the optimized structures are shown in Table 4.

The fingerprint plots of the **mF₁** and **26dF₁** molecules show a singular feature near the (*d*_i = 2.4 Å, *d*_e = 2.0 Å) point. This

Table 4. Interaction Energy Values (*E_w*) for **26dF₁** in Contact with Water Molecules Estimated with *CRYSTAL* at the DFT(B3LYP)/6-31G(d,p) Level of Theory Together with Geometrical Parameters of Hydrogen Bond O–H...O Interactions (Optimal Geometry)^a

motif	<i>E_w</i> /kJ·mol ^{−1}	<i>d</i> _{O...H} (Å)	<i>d</i> _{H...O} (Å)	<i>d</i> _{O...O} (Å)	θ _{O–H...O} (°)
W1	−17.7	0.984	1.735	2.706	168.4
W2	−28.1	0.989	1.710	2.693	171.9
W3	−35.7	0.989	1.724	2.702	169.3
W4	−19.7	0.984	1.747	2.719	168.9

^aSchematic representation is given above the table.

represents the regions on the Hirshfeld surface corresponding to the noninteractive fluorine and hydrogen atoms contacts. In general, the Hirshfeld surface plot of the **26dF₁** structure is very similar to that of **mF₁**. There are only some small discrepancies noticeable in the related fingerprint plots. The relatively sparse distribution of points visible on the **26dF₁** fingerprint plot, in-between the pair of the O...H spikes, corresponds to the close H...H distances across boronic acid cyclic dimers. Similar observation was reported for carboxylic acids.^{20c,d} However, quite surprisingly, those features mostly disappear when the structure is optimized (Figure 5S in Supporting Information). This may suggest that in this case this is rather an artifact of the IAM model employed in the structure refinement. It should be noted that the investigation does not support the formation of any significant weak interactions involving fluorine and boron atoms. In addition, the volume of the **26dF₁** unit cell is larger by about 20 Å³, than for the **mF₁**, which suggests a less efficient packing in the former case.

CRYSTAL computations confirm the comparable stability of both isomorphous forms (−273 kJ·mol^{−1} for **mF₁** and −267 kJ·mol^{−1} for **26dF₁**). The **mF₁** structure seems to be slightly more advantageous than **26dF₁**. This might result from its less compact packing which was mentioned before. Longer intermolecular distances are probably caused by the fluorine atoms. The fluorine atoms desire more space than hydrogen

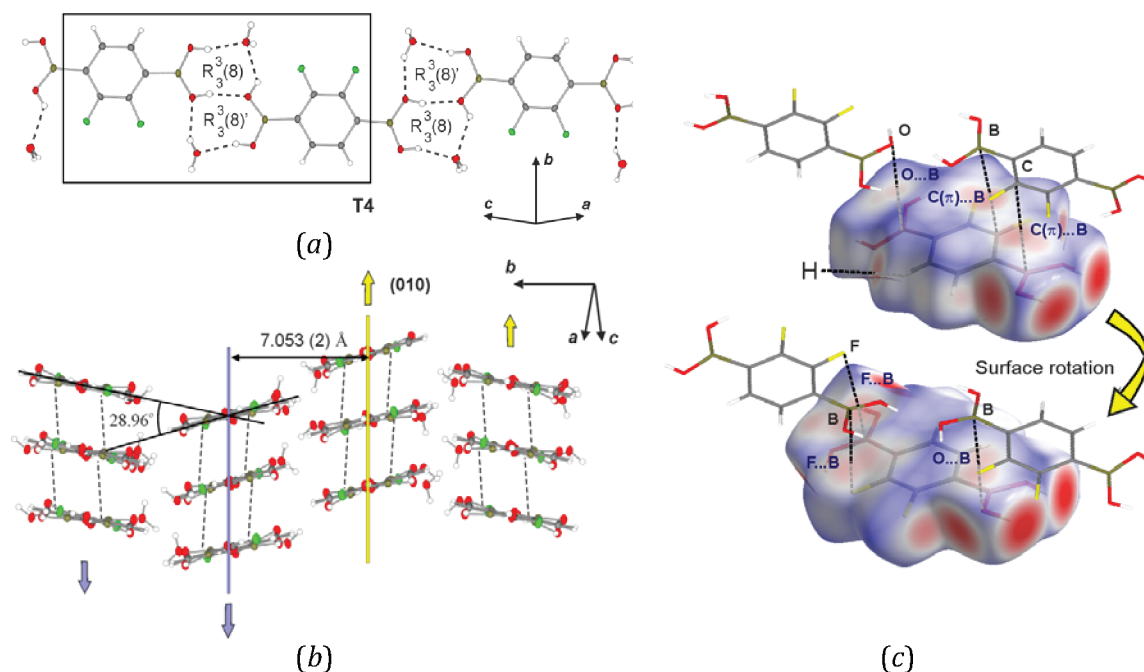


Figure 6. (a) Molecular chain constructed by the 23dF₂ diboronic acid and water molecules. (b) Packing diagram showing how the weak C(π)⋯B, F⋯B, and O⋯B interactions (marked as dashed lines) participate in the formation of the 2D layers. (c) Hirshfeld surface for the 23dF₂A molecule depicted with some weak interactions.

atoms and also influence the molecular charge distribution. This, in turn, affects the geometry and molecular assembly. The 26dF₁, which contains two fluorine substituents in a diboronic acid molecule, is thus less tightly surrounded by other moieties in its crystal lattice. On the other hand, it seems that longer interatomic contacts do not hamper the interaction strength between acid molecule dimers building the crystal network. Indeed, despite the example of the D1 dimer, the cohesive energies evaluated for the waterless mF₁ and 26dF₁ hypothetical forms (i.e., the same geometry and structural parameters but with solvent moieties excluded) are also very much alike (about 112 kJ·mol^{−1}). This suggests that there is a balance between the fluorine atom effect and diboronic acid intermolecular distance, leading to the similar stabilization strength. The overall cohesive energy difference must then come from a subtle dissimilarity in the interactions with the solvent species. Less compact diboronic acid arrangement in the 26dF₁ structure may preserve the interactions in the diboronic acid net. However, due to the longer intermolecular distances this may lead to less efficient interactions with water moieties, affecting the cohesive energy value.

As a supplementation of the whole structural discussion concerning the two isomorphous compounds, a CSD search was carried out, leading to an interesting finding. It appears that the supramolecular patterns described for the structures of mF₁ and 26dF₁ are very similar to those found for a pseudopolymorphic form of 4-carboxyphenylboronic acid.²¹ Fairly similar unit cell parameters and 3D arrangements, in which water molecules span hydrogen-bonded chains, make the three structures identical from the topological point of view. The only difference is the internal symmetry of the crystal. While the structures of mF₁ and 26dF₁ crystallize in the centrosymmetric *Cccm* space group, the carboxylic acid adopts a non-centrosymmetric *Ccc2* one. This is mainly because the adjacent molecules are held by hydrogen bonds formed between boronic and carboxylic groups; therefore there is no center of symmetry. Clearly, an

addition of the inversion center into the *Ccc2* space group transforms it directly into *Cccm*. However, it is worth noting that due to low data quality it is hardly possible to judge if the apparent *Ccc2* space group symmetry is the right one. The improper assignment of hydrogen atoms, a possible disorder of the whole acid moiety, and the high temperature of the measurement cause serious doubts concerning the structure reliability and may rather indicate the higher *Cccm* symmetry of the crystal lattice. This suggestion, in fact, is supported by the CHECKCIF report. Unfortunately it was impossible to verify these suppositions in the absence of the structure factor data.

3.4. Supramolecular Structure of 23dF₂. The 23dF₂ constitutes another fluorine diboronic acid derivative characterized by the increased water content in its crystal lattice. The asymmetric part of the unit cell contains two molecules of diboronic acid (23dF₂A and 23dF₂B) and four water molecules. No disorder is observed within the B(OH)₂ moiety and fluorine atoms. Both boronic groups in the first molecule (bound to C1 and C7 carbon atoms) adopt a *syn*–*syn* conformation. In the second molecule the *syn*–*anti* conformations are observed (for the B(OH)₂ groups bound to C4 and C10 centers). The supramolecular structure of 23dF₂ is the most distinct one from all other structures described so far in this manuscript. Because of the presence of numerous intermolecular hydrogen bond interactions, supramolecular assembly is based on a quite complex pattern of hydrogen-bonded network. In contrast to the remaining diboronic acids, molecular chains in 23dF₂ are not held by typical centrosymmetric R₃²(8) dimers. Instead, molecules of diboronic acid are mutually displaced and form chains (along the [101] crystal direction), in which water molecules constitute a kind of a molecular glue (Figure 6a). Within the chains, the molecules of 23dF₂A and 23dF₂B are in the interspersed arrangement and interact one with another via single hydrogen bonds only (dimer D1'). The second boronic hydroxyl group is engaged in hydrogen interaction with water molecules, two of which (O9 and O11)

act as single donors and single acceptors, whereas the O10 and O12 ones are double acceptors of hydrogen bonds. Similarly skewed architectures of diboronic chains are rare and have been solely observed for the structure of bis(4-boronicphenyl)-acetylene.^{2h} The chains associate further by the interactions between the B(OH)₂ groups and water molecules, supported by the water–water contacts. In summary, each of the four symmetrically independent water molecules is engaged in three O–H···O interactions with the boronic fragments, linking diboronic acids within and in-between chains, and also participates in one interaction with another water molecule.

The Hirshfeld surfaces for both symmetry-independent molecules of **23dF₂** have very similar shape and interaction patterns. Eight substantial hotspots belong to the strong O–H···O interactions, and they are represented as a symmetric pair of spikes in the fingerprint plots. The hydrogen-bonded framework is reinforced by much weaker, dispersive interactions. Strong Lewis acidity of boron atom in its three-coordinated state attracts more electronegative partners such as oxygen and fluorine atoms but also the π -densities. Several bright red spots located at the both sides of the Hirshfeld surface are clearly visible. These arise from the C(π)···B and O···B interactions and contribute to the relatively dense distribution of points on fingerprint plots. The other important spot related to the boron atom is recognized as the F···B interaction and is located near the ($d_e = 1.7$ Å, $d_i = 1.5$ Å) point in the adequate fingerprint plot. The molecules of **23dF₂A** and **23dF₂B** belonging to parallel chains are paired due to the self-complementary of C(π)···B ($d_{C6\cdots B4} = 3.209$ Å, $d_{C9\cdots B1} = 3.219$ Å) and F···B interactions ($d_{F3\cdots B2} = 3.127$ Å, $d_{F2\cdots B3} = 3.195$ Å). As a result of these weak contacts the **23dF₂** molecules form **D3** dimers, similar to the ones observed for the **noFb₀** and **25dF₀** structures. However, unlike in **23dF₂**, the weak C(π)···B interactions in **noFb₀** and **25dF₀** arise symmetrically from both sides of the molecule, while in the case of **23dF₂** one side is arranged in C(π)···B contacts and the other in F···B contacts (Figure 6c). There is also a quite intensive spot visible on the Hirshfeld surface, which corresponds to a very short H···H distance of 2.270(2) Å between aromatic hydrogen atoms of **23dF₂A**. This contact is represented by a sharp spike along the diagonal at $d_e = d_i = 1.1$ Å. It is notable that for the second molecule from the asymmetric unit, **23dF₂B**, the corresponding spike is much shorter and bulged, which indicates a longer H···H distance.

All the strong O–H···O and weak C(π)···B, F···B, and O···B interactions have a great contribution to the supramolecular structure stabilization. The association of hydrogen-bonded chains by weak interactions involving boron atom, within the **D3** dimers, and lateral hydrogen contacts from dimeric water units, leads to the formation of molecular layer (propagating parallel the (010) crystal plane) as it is shown in Figure 6b. The 3D structure has a double-layered herringbone architecture with the interlayer distance equal to 7.053 Å and the bond angle between the mean square planes of nonparallel molecules from adjacent layers equal to 28.96°. We suppose that the role of water in this structure, as well as in the other structures of diboronic acids, goes beyond the hydrogen-bonded architecture building unit. In accordance with theoretical calculations, water molecules allow for optimizing the interactions between electronegative atoms or aromatic π -electrons and boron atom.

The complexity and effectiveness of molecular packing of **23dF₂** in the crystal lattice is reflected in the low cohesive energy value, which amounts to -648 kJ·mol⁻¹ per asymmetric

unit. This makes -324 kJ·mol⁻¹ on average per one diboronic acid molecule and two water molecules, and is about 70 kJ·mol⁻¹ lower than the corresponding values for **mF₁** and **26dF₁** (Table 2). Such an energy difference, with respect to the **mF₁** and **26dF₁** crystal structures, results from the presence of the additional water molecule, being an extra hydrogen bonding donor and acceptor. On the other hand, the anhydrous structure stabilization energy of **23dF₂** is substantially less profitable than in the case of **mF₁** and **26dF₁** (-91.1 kJ·mol⁻¹ and about -112 kJ·mol⁻¹, respectively). This is because diboronic acid molecules are less compactly arranged in the crystal lattice of **23dF₂** as some space is dedicated for water molecules. Therefore, the distance between chains is greater and boronic acid groups adopt more stable, as indicated by single point calculations (Figure 2), almost flat conformation, lying in the aromatic ring plane. Such an arrangement of the acid species reduces their mutual interaction. However, the π -stacking contacts between the two neighboring molecular layers are more efficient, when compared to the corresponding interactions observed for the other studied systems (Table 3, dimers **D3** and **D3'**).

The cohesive energy computation results show the vast impact of water molecules on the overall crystal lattice stabilization. The energetic gain due to the presence of solvent species amounts to over 450 kJ·mol⁻¹ per asymmetric unit (i.e., the difference between the cohesive energy derived for the studied crystal and its waterless analogue). The solvent effect on crystal structure stabilization energy is illustrated by the example of **D1'** dimer and **T4** arrangement (Figure 6a), which is composed by two diboronic acids and two water molecules. The contribution from water molecules to the **T4** stabilization energy reaches about 115 kJ·mol⁻¹, which shows the scale of the solvent effect. Similar to the other examined structures containing water molecules, the strength of the hydrogen bond between boronic acid and water molecule is greater when that water molecule constitutes a boronic acid proton acceptor.

3.5. Supramolecular Structure of noFa₄. This particular structure was reported by Höpfl et al.²¹ Therefore, here we just give a brief description of its supramolecular architecture and analyze the patterns of intermolecular interactions in order to provide a comprehensive picture supplementing our study. The **noFa₄** compound crystallizes in the triclinic $\bar{P}1$ space group with four molecules of water per one molecule of diboronic acid, which constitutes the highest water content in the crystal lattice among the examined systems.

As observed in the other studied systems, except for **23dF₂**, the main pattern in the crystal lattice of **noFa₄** is the one-dimensional (1D) molecular chain constructed by the centrosymmetric R₂²(8) motifs involving the B(OH)₂ groups (**D1** dimer). These associate further by weak C(π)···B and O···B interactions (**D3** motif) forming a molecular layer parallel to the ($\bar{1}13$) crystal plane (Figure 7b). Weak interactions are well visible as bright spots on the Hirshfeld surface (Figure 7a). The molecular arrangement is similar to the ones found in **noFb₀**, **25dF₀**, and **23dF₂**. However, in the case of **noFb₀** and **25dF₀** boronic groups are significantly rotated with respect to the aromatic ring planes, which leads to the formation of the undulated 2D molecular layers of diboronic acid chains joined via side hydrogen bonds. In the case of **noFa₄**, the chain motifs are connected with the water mediated hydrogen bonding, increasing the dimensionality of the system. Consequently, **noFa₄** exhibits a 3D structure formed by the layers of diboronic acids intercalated by the layers of water molecules (Figure 7b).

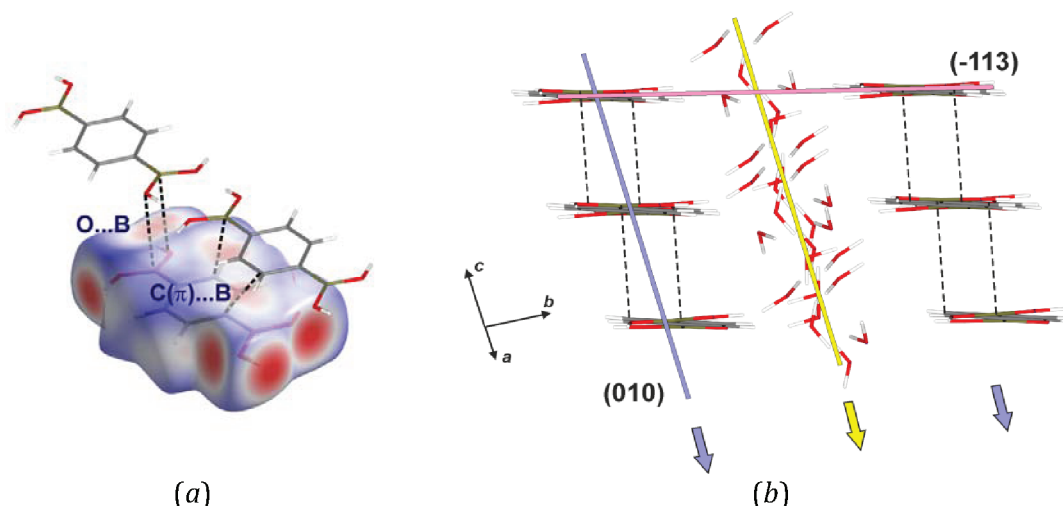


Figure 7. (a) Hirshfeld surface obtained for the **noFa₄** structure shown with selected neighboring molecules and weak interactions. (b) Packing diagram showing selected adjacent layers (blue and yellow arrows show the layer propagation) of diboronic acid and water molecules.

Such arrangement allows molecules of diboronic acid for adopting a more stable, flat conformation.

Computational studies show that, as it was in the case of **23dF₂**, the waterless structure of **noFa₄** is characterized by the cohesive energy greater than that obtained for other systems containing lower amounts of water in their structures. This is due to a more dispersed crystal packing of **noFa₄**. Although there is much more space between the neighboring chain motifs lying in the same plane parallel to the ($\bar{1}13$) crystal plane, so as to accommodate the water species, the distance between parallel dispersively interacting chains is smaller than the corresponding values for **noFb₀** and **25dF₀**, and amounts to 3.284 Å. Consequently, the interaction between 2D layers is equal to $-89.9 \text{ kJ}\cdot\text{mol}^{-1}$ and is lower than that for **noFb₀** and **25dF₀**. The stabilization energy of D1 motif is comparable to the results obtained for the same structural motif observed in the other studied systems. The D3 dimer, in turn, seems to be slightly better stabilized than in the other cases, except for **23dF₂**. The D3 dimer interaction energy results for **23dF₂** and **noFa₄** suggest that the π -stacking contacts are more efficient when boronic groups lie in the aromatic ring planes as then the interacting molecules may adopt closer arrangement in space which provides a better π -covering. It also seems that the presence of fluorine atoms usually increase the strength of such interactions.

The total cohesive energy per asymmetric unit amounts to $-420.4 \text{ kJ}\cdot\text{mol}^{-1}$ for the **noFa₄** crystal structure. The same quantity for its waterless analogue equals $-91.0 \text{ kJ}\cdot\text{mol}^{-1}$. This means that the total energy gain due to the presence of water molecules is of about $329 \text{ kJ}\cdot\text{mol}^{-1}$ in magnitude. The stabilization energy of diboronic acid interacting with four surrounding water molecules is also significant ($-98 \text{ kJ}\cdot\text{mol}^{-1}$). It is worth stressing here that in general each additional water molecule lowers the crystal cohesive energy with a smaller impact. One water molecule in **mF₁** and **26dF₁** increases the crystal stability of over $150 \text{ kJ}\cdot\text{mol}^{-1}$ with respect to the nonsolvent case. In turn, in the case of **23dF₂**, two water molecules lower the cohesive energy of $250 \text{ kJ}\cdot\text{mol}^{-1}$ on average, which means that about $125 \text{ kJ}\cdot\text{mol}^{-1}$ per a solvent moiety. Finally for **noFa₄** the impact of each water molecule is reduced to about $80 \text{ kJ}\cdot\text{mol}^{-1}$.

In the **noFa₄** structure, it was also possible to compute the interlayer interaction energies between slabs containing water molecules. As illustrated in Figure 7b, there are well visible molecular layers parallel to the (010) crystal planes. Computational result for the stabilization energy of such diboronic acid–water slabs showed once again the importance of the solvent content. This interaction reaches $-187.8 \text{ kJ}\cdot\text{mol}^{-1}$ per a unit cell and reflects the interaction strength between diboronic acid and water species.

4. COMPARATIVE REFLECTION AND CONCLUSIONS

The studied series of diboronic acid derivatives constitutes a structural continuum of differently hydrated architectures. However, at the same time, it might be considered as a sequence of diboronic acid modifications gradually enriched in the fluorine content. Therefore, particular attention should be paid to these two leading aspects, that is, water incorporated in the crystal lattice and fluorine substituents, and their influence on the spatial arrangement of molecules in the resulting crystal networks.

Together with the growing number of water molecules per acid moiety, we observe the stepwise alternation of the crystal packing, starting from the layered aggregation in **noFb₀**, **25dF₀**, and **tF₀**, through the catenated network in isostructures **mF₁** and **26dF₁**, ending with the double-herringbone packing and alternate layers of diboronic acid and water molecules for **23dF₂** and **noFa₄**, respectively. As indicated by the theoretical calculations performed in the CRYSTAL and PIXEL programs, the general trend is that diboronic acid structures containing a greater amount of water are better stabilized (Table 2). Indeed, in all of the studied crystal structures the main structural motifs are based on hydrogen bonds, and the presence of water molecules provides the increased number of this kind of intermolecular contact. This is reflected in the augmented contribution of the electrostatic and polarization components to the total crystal lattice stabilization energy. PIXEL results revealed that in the case of **noF**, **25dF₀**, and **tF₀** the polarization energy component is less significant than the dispersive energy contribution, while the electrostatic energy value is the most substantial one. In turn, in the case of **mF₁** and **26dF₁** the polarization energy component strongly outnumbers the dispersive energy value. These two are also characterized by

much more stabilizing electrostatic interactions than **noFb₀**, **25dF₀**, and **tF₀** (over 160 kJ·mol⁻¹ more advantageous). The percentage contributions of hydrogen bond contacts to the overall stabilization energy ranges from about 60% for the anhydrous group and **mF₁** and **26dF₁**, through 65% for **23dF₂**, to nearly 75% for **noFa₄**. The average strength of hydrogen bonding amounts to 24–28 kJ·mol⁻¹. This indicates that hydrogen bonds are slightly stronger when water–water contacts are enabled.

The most important synthons formed via hydrogen bonding contacts are R₂²(8) and R₂²(16), which correspond to the **D1** and **D2** dimers. The average strengths of **D1** and **D2** dimer interactions are about -40 to -50 kJ·mol⁻¹. These energy values are comparable to the binding energies of other boronic acid dimers reported in the literature (-50.2 kJ·mol⁻¹ for the HB(OH)₂ dimer²² and -50.5 kJ·mol⁻¹ for the NH₂-CH₂-B(OH)₂ dimer²³ both calculated at the MP2/6-311G(d,p) level of theory, and -49.4 kJ·mol⁻¹ for phenylboronic acid dimer^{2c} at MP2/6-31G(d,p)). The **D1** dimer is formed in each structure, except for **23dF₂**. In the latter case we observe dimers consisting of mutually shifted diboronic acids (**D1'**), where the interaction between two acid molecules is weaker. The **D1'** motif is then additionally stabilized from the sides with the aid of water molecules. In turn, the **D2** motif is characteristic for the anhydrous structures, where hydrogen bonded chains are linked together from the sides via hydrogen bonding created between the acid molecules. In the water-containing structures, the space around diboronic acid chain motifs is filled with different water arrangements.

The second aspect concerns the fluorine substitution of the aromatic ring and its influence on the diboronic acid binding properties. As shown by Hirshfeld surface analysis and the theoretical calculations, the C–H···F and F···F contacts do not directly participate in the composition of the crystal lattice. This is especially noticeable in the structures of **mF₁** and **26dF₁**, where the network is dominated by strong hydrogen interactions and does not include any significant weak interactions involving fluorine atoms. This is supported by the fact that the fluorine atoms are disordered and can occupy each site at the aromatic ring with equal probability. It is also important to note that the additional fluorine atom does not affect the stabilization of the **D1** hydrogen-bonded dimers significantly. The direct contacts involving fluorine atoms are also absent in the structure of **25dF₀**, which is isostructural to **noFb₀**. Furthermore, only in the case of **23dF₂** and **tF₀** (**D3'** and **D3''** dimer, respectively) direct interactions employing the fluorine atoms (F···B contacts) are observed.

As mentioned before, a significant twisting of the B(OH)₂ group in **noFb₀**, **25dF₀**, and **tF₀** leads to more efficient contacts between adjacent acid molecules and thus to more compact packing. The more advantageous values of the **D2** dimer interaction energies in **tF₀** and **noFb₀** are partially counterbalanced by the less stable molecular conformation (boronic groups are more twisted). The lower stability of the boronic acid conformation is caused by weaker conjugation of the twisted boronic group with the aromatic ring, and also by weaker intramolecular hydrogen O–H···F or/and C–H···O contacts. In contrast, two intramolecular O–H···F and two C–H···O contact types present in **25dF₀** hamper the rotation of the boronic group and stabilize the flat conformation. Consequently, this molecule is to a less extent distorted from planarity, and thus the **D2** dimer is less efficiently stabilized. A substantially different effect is found for the other studied

compounds. In the case of the **mF₁** and **26dF₁** monohydrates, a high value of the τ angle enables optimal contacts with water molecules. In the structures with a higher water content (**23dF₂**, **noFa₄**), the molecules of diboronic acids are no longer arranged in the side contact patterns. Therefore, there is much more space around chain motifs, which enables acid groups to adopt a more energetically stable planar conformation (with respect to aromatic rings). It is worth noting here that this flat conformation allows for a stronger π -stacking interactions observed for the **D3** type dimer. Additionally, in the case of the **23dF₂** and **noFa₄** structures, water molecules can interact one with another. This, in turn, supports formation of the effective weak interaction network, where more than one water molecule per one acid moiety is present.

Having a closer look at the proton disorder within boronic group, it seems that it is also ruled by intramolecular interactions with fluorine atoms. In the **25dF₀** structure, the position of the fluorine atoms is well-defined as a result of the complementary C–H···O and C–F···H–O intramolecular contacts. This is also true for the **23dF₂** derivative, where the positions of the hydrogen atoms are determined by directional interactions with the water molecules. For the more symmetric **tF₀** derivative, the intramolecular interactions are weaker. Moreover, there is no side preference (i.e., two fluorine atoms are always in *ortho* positions). In the case of **mF₁** and **26dF₁** derivatives, the fluorine atoms are systematically disordered (Figure 8). However, without multitemperature neutron or

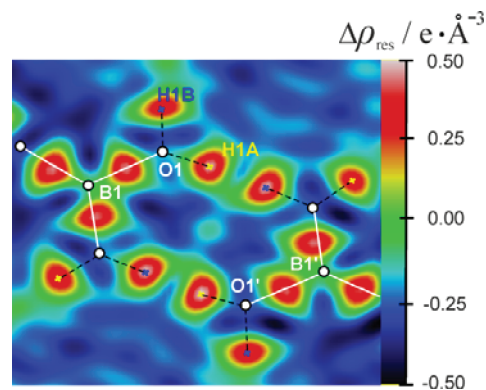


Figure 8. Residual density map for the **D1** dimer moiety in **26dF₁** (reconstructed without hydrogen atoms on OH groups). Proton disorder is clearly visible.

X-ray high-resolution data, we cannot justify whether the observed proton disorder is static or dynamical in nature, and how it is governed by the intramolecular interactions. More detailed studies on that matter for similar dimers have been performed recently for carboxylic acids.²⁴

In conclusion, the above results suggest that the C–H···F and F···F contacts are being avoided. In other words, they do not participate directly in the formation of a crystal lattice. Nevertheless, the packing motifs discussed here indicate some trends in the formation of the F···B interactions, which contributes to the specific understanding of the influence of fluorine interactions, particularly in the presence of boron atoms. Moreover, the role of a fluorine atom goes beyond the directional impact on the structural stabilization. The geometry change resulting from the fluorine substitution is reflected, for example, in the **D2** dimer stabilization energies, or in the strength and character of boronic acid contacts with water

molecules. Fluorine atoms affect the torsion angle of a boronic group by stabilizing/destabilizing contacts between an OH group and hydrogen/fluorine atoms. Additionally, our work shows and, to some extent explains, the substantial role of the solvent molecules incorporated into a crystal lattice.

5. EXPERIMENTAL SECTION

5.1. Materials and Synthesis. All reactions were carried out under an argon atmosphere. Solvents were stored over sodium wire before being used. *n*-Butyllithium (10 M solution in hexanes), diisopropylamine, and triisopropyl borates were used as received without further purification. ^1H and ^{13}C NMR chemical shifts are given relative to TMS using residual solvent resonances. ^{11}B and ^{19}F NMR chemical shifts are given relative to $\text{BF}_3\cdot\text{Et}_2\text{O}$ and CFCl_3 .

Fluoro-1,4-phenylenediboronic Acid (mF). A solution of *n*BuLi (10 M, 2.0 mL, 20 mmol) was added to the stirred solution of 1,4-dibromo-2-fluorobenzene (5.10 g, 20 mmol) in Et_2O (20 mL) at -80°C . After ca. 30 min a mixture containing the lithium derivative was quenched with $\text{B}(\text{OiPr})_3$ (4.61 mL, 20 mmol). The mixture became thick, and therefore, it was diluted with an additional 20 mL of THF. The mixture was allowed to warm to -60°C and then, after another 30 min of stirring at this temperature, the solution of *n*BuLi (10 M, 2.0 mL, 20 mmol) was added, followed by the addition of a second portion of $\text{B}(\text{OiPr})_3$ (4.84 mL, 21 mmol). After ca. 1 h of stirring at -60°C the mixture was warmed to -30°C and quenched with 2 M ethereal solution of HCl (21 mL). The mixture became clear. At 20°C water was added, white precipitate appeared and it was filtered. Resulting powder was washed with Et_2O and water and dried to give the title compound. Yield, $y = 2.70$ g (72%); melting point temperature, $T_m > 350^\circ\text{C}$. ^1H NMR ($[\text{D}_6]$ acetone, 400 MHz): $\delta = 7.71$ (t, $J = 7.2$ Hz, 1 H, Ph), 7.39 (d, 1 H, Ph), 7.39 (s, 2 H, $\text{B}(\text{OH})_2$), 7.21 (d, $J = 2.4$ Hz, 2 H, $\text{B}(\text{OH})_2$), 3.09 (s, 2 H, H_2O) ppm. $^{13}\text{C}\{^1\text{H}\}$ NMR ($[\text{D}_6]$ acetone, 100.6 MHz): $\delta = 167.5$ (d, $J = 243.9$), 136.6 (d, $J = 7.6$ Hz), 130.1 (d, $J = 2.2$ Hz), 120.4 (d, $J = 22.8$ Hz). ^{11}B NMR ($[\text{D}_6]$ acetone, 64.16 MHz): $\delta = 28$ ppm. $\text{C}_6\text{H}_4\text{B}_2\text{FO}_4\cdot\text{H}_2\text{O}$ (201.75): calculated: C (39.22), H (3.84); found: C (39.13), H (3.92).

2,5-Difluoro-1,4-phenylenediboronic Acid (25dF). Compound was prepared as described for mF, starting with 1,4-dibromo-2,5-difluorobenzene, except that the first step of the reaction was accomplished with an in situ technique (to the solution of substrate and $\text{B}(\text{OiPr})_3$, 2M *n*BuLi was added). Moreover, THF instead of Et_2O was used as solvent, and all lithiation/boronation steps were performed at -90°C . The resultant mixture was hydrolyzed with 1.5 M aqueous H_2SO_4 (15 mL) at -10°C . The water phase was separated and followed by extraction with diethyl ether (2×15 mL). The extracts were added to the organic phase, which was concentrated under reduced pressure. A solid residue was filtered and washed consecutively with water (2×10 mL) and hexane (5 mL). Drying in vacuo afforded the title compound as a white powder. $T_m = 214 - 215^\circ\text{C}$. ^1H NMR ($[\text{D}_6]$ DMSO, 400 MHz): $\delta = 8.34$ (s, 4 H, $\text{B}(\text{OH})_2$), 7.16 (t, $J = 6.4$ Hz, 2 H, Ph) ppm. $^{13}\text{C}\{^1\text{H}\}$ NMR ($[\text{D}_6]$ DMSO, 100.6 MHz): $\delta = 169.2$ (d, $J = 23.2$ Hz), 130.1 (dd, $J = 247.27$ Hz, $J = 11.4$ Hz). ^{11}B NMR ($[\text{D}_6]$ DMSO, 64.16 MHz): $\delta = 28$ ppm. $\text{C}_6\text{H}_2\text{B}_2\text{F}_2\text{O}_4$ (201.73): calculated: C (35.72), H (3.00); found: C (35.66), H (2.94).

Tetrafluoro-1,4-phenylenediboronic Acid (tF). A solution of lithium diisopropylamide (LDA) freshly prepared from diisopropylamine (10.10 g, 100 mmol) and *n*BuLi (10 M, 10.0 mL, 100 mmol) was added to a stirred solution of 1,2,4,5-tetrafluorobenzene (7.5 g, 50 mmol) containing $\text{B}(\text{OiPr})_3$ (14.6 g, 100 mmol) in THF (70 mL) at -80°C . White slurry was formed. After about 30 min the mixture was allowed to warm to -30°C . Then it was quenched with 2 M ethereal solution of HCl (50 mL), warmed to room temperature, and 2 M aq. solution of HCl was added. The water phase was separated followed by extraction with ether (2×15 mL). The extracts were added to the organic phase, which was concentrated under reduced pressure. Drying in vacuo afforded the title compound as a white powder, $T_m = 184 - 186^\circ\text{C}$. ^1H NMR ($[\text{D}_6]$ DMSO, 400 MHz): $\delta = 8.08$ (s, 4 H, $\text{B}(\text{OH})_2$) ppm. $^{13}\text{C}\{^1\text{H}\}$ NMR ($[\text{D}_6]$ DMSO, 100.6 MHz): $\delta = 147.5$ (d, $J = 233.5$). ^{11}B NMR ($[\text{D}_6]$ DMSO, 64.16 MHz):

$\delta = 28$ ppm. ^{19}F NMR ($[\text{D}_6]$ DMSO, 376.47 MHz): $\delta = -133.5$ ppm. $\text{C}_6\text{H}_2\text{B}_2\text{F}_4\text{O}_4$ (237.71): calculated: C (30.32), H (1.70); found: C (30.43), H (1.59).

5.2. Crystallization. Single crystals of the studied compounds and their hydrates were prepared by crystallization of the compounds from an appropriate solvent. The crystals of tF and 25dF were obtained as pure forms upon crystallization from 2:1 toluene/acetone solution. The crystals of hydrates mF and 26dF were obtained by slow evaporation of appropriate acetone solutions, while the crystallization from 1:1 acetone/water solution gives single crystals of 23dF. Nevertheless, applying different crystallization conditions (various solvents, evaporation surfaces, etc.), we did not manage neither to obtain pure forms of mF, 26dF, and 23dF, nor hydrates of 25dF and tF.

5.3. Crystal Structure Determination. X-ray diffraction data sets for single crystals of mF, 25dF, tF were collected at 100 K on a Bruker AXS Kappa APEX II Ultra diffractometer with a TXS rotating anode (Mo- K_α radiation, $\lambda = 0.71073$ Å), multilayer optics and equipped with an Oxford Cryosystems nitrogen gas-flow attachment. The data collection strategy was optimized and monitored using the appropriate algorithms applied in the APEX2 program package.²⁵ Data reduction and analysis were carried out with the APEX2 suite of programs (integration was done with SAINT²⁶). The multiscan absorption correction, scaling, and merging of reflection data were done with SORTAV.²⁷ Single crystals of 26dF and 23dF were measured on a Kuma KM4CCD κ -axis diffractometer with graphite-monochromated Mo- K_α radiation and equipped with an Oxford Cryosystems nitrogen gas-flow apparatus. Data reduction and analysis were carried out with the Oxford Diffraction Ltd. suite of programs.²⁸ All structures were solved by direct methods using SHELXS-97 and refined using SHELXL-97.²⁹ Selected crystal data for all crystals are summarized in Table 5. In the case of mF and 26dF, it was necessary to include a disorder model with fluorine and aromatic hydrogen atoms. The site occupancy factors of fluorine atoms were fixed at the exact values of 0.25 and 0.50 for mF and 26dF, respectively. Other details are available from the Supporting Information.

5.4. Computational Methods. (a). *Single-Point Calculation with GAUSSIAN.*³⁰ The single-point calculations were performed within the second-order Møller–Plesset (MP2) approximation.¹⁸ Dunning–Woon aug-cc-pVTZ,¹⁹ basis sets were used throughout. The single-molecule constrained energy scan of C2–C1–B1–O1 dihedral angle was also performed at the MP2/aug-cc-pVTZ level of theory. During the scan procedure only the dihedral angle C2–C1–B1–O1 was constrained and all other parameters were fully optimized. During the calculations no symmetry constraints were applied.

(b). *CRYSTAL Calculations.* All energy computations within the CRYSTAL09 program package¹⁵ were performed at the DFT-(B3LYP)³¹ level of theory. 6-31G(d,p)³² molecular all-electron basis set occurred to be sufficient for the purpose of the conducted calculations. Both Grimme dispersion correction³³ and correction for the basis set superposition error were applied. Ghost atoms were selected up to 5 Å distance from the studied molecule in a crystal lattice and were used for the basis set superposition error estimation. The evaluation of Coulomb and exchange series was controlled by five thresholds, set arbitrary to values of 10^{-7} , 10^{-7} , 10^{-7} , 10^{-7} , 10^{-25} . The condition for the SCF convergence was set to 10^{-7} on the energy difference between two subsequent cycles. Shrinking factor was equal to 4, which refers to 30–36 k-points (depending on space group symmetry) in the irreducible Brillouin zone in the case of the studied systems and assures the full convergence of the total energy. Two types of coordinates were used. First, molecular geometries were taken directly from the X-ray structural data analysis, while all X–H bonds were fixed at standard neutron distances. Then, all the structures were optimized with CRYSTAL and they served for the subsequent energy calculations. In the case of the structures, which exhibit layer architectures, the same two sets of coordinates were subjected to crystal interlayer interaction computations. The majority of the calculation parameters were set identical as for the purpose of the cohesive energy determination. The only difference was in ghost atom definitions. Here, an additional upper and lower molecular layers were used as ghost functions for appointing the basis set superposition error.

Table 5. Selected Crystal Data, Data Collection and Refinement Parameters for Measured 1,4-Phenylenediboronic Acids

	mF ₁	26dF ₁	23dF ₂	25dF ₀	tF ₀
formula	C ₆ H ₂ B ₂ F ₄ O ₄ ·H ₂ O	C ₄ H ₆ B ₂ F ₂ O·H ₂ O	C ₆ H ₆ B ₂ F ₂ O ₄ ·2H ₂ O	C ₆ H ₆ B ₂ F ₂ O ₄	C ₆ H ₄ B ₂ F ₄ O ₄
molecular mass, <i>M_r</i> (a.u.)	201.75	219.74	237.76	201.73	237.71
temperature, <i>T</i> (K)	100(1)	100(1)	100(1)	100(1)	100(1)
crystal system	orthorhombic	orthorhombic	monoclinic	triclinic	monoclinic
space group	<i>Cccm</i>	<i>Cccm</i>	<i>P2₁/c</i>	<i>P</i> $\bar{1}$	<i>P2₁/n</i>
<i>a</i> (Å)	12.049(1)	12.207(2)	9.551(1)	4.984(2)	8.426(1)
<i>b</i> (Å)	7.277(1)	7.329(1)	28.212(2)	5.257(2)	5.024(1)
<i>c</i> (Å)	10.055(1)	10.081(2)	7.652(1)	7.423(3)	10.166(1)
α (°)	90	90	90	74.67(1)	90
β (°)	90	90	109.57(1)	84.64(1)	106.25(1)
γ (°)	90	90	90	89.00(1)	90
volume, <i>V</i> (Å ³)	881.7(1)	901.9(3)	1942.7(2)	186.7(1)	413.2(1)
<i>Z</i>	4	4	8	1	2
<i>d</i> _{calc} (g·cm ^{−3})	1.520	1.618	1.626	1.794	1.911
<i>F</i> (000)	416	448	976	102	236
θ range (°)	24.22	28.58	28.58	28.16	24.22
absorption coefficient, μ (mm ^{−1})	0.137	0.156	0.159	0.171	0.204
index ranges	−17 ≤ <i>h</i> ≤ 16 −10 ≤ <i>k</i> ≤ 10 −14 ≤ <i>l</i> ≤ 11	−16 ≤ <i>h</i> ≤ 16 −9 ≤ <i>k</i> ≤ 9 −13 ≤ <i>l</i> ≤ 13	−12 ≤ <i>h</i> ≤ 12 −36 ≤ <i>k</i> ≤ 37 −10 ≤ <i>l</i> ≤ 10	−7 ≤ <i>h</i> ≤ 6 −6 ≤ <i>k</i> ≤ 5 −10 ≤ <i>l</i> ≤ 9	−10 ≤ <i>h</i> ≤ 8 −5 ≤ <i>k</i> ≤ 6 −13 ≤ <i>l</i> ≤ 13
no. of reflections collected/unique	6042/3740	8047/610	36210/4779	2255/901	3774/947
<i>R</i> _{int} (%)	2.21	2.15	2.54	4.30	4.12
no. of parameters/restraints	51/3	51/3	289/0	64/0	86/4
GOF	1.135	1.086	1.043	1.073	1.109
<i>R</i> [<i>F</i>]/ <i>wR</i> [<i>F</i> ²] (<i>I</i> > 2σ(<i>I</i>))	4.03%/11.90%	3.02%/8.90%	3.52%/10.67%	6.45%/17.19%	5.54%/16.08%
<i>R</i> [<i>F</i>]/ <i>wR</i> [<i>F</i> ²] (all data)	4.53%/12.26%	3.70%/9.13%	5.31%/11.15%	9.40%/19.88%	7.58%/17.25%
max and min residual density/e·Å ^{−3}	+0.51/−0.26	+0.47/−0.21	+0.42/−0.33	+0.56/−0.53	+0.48/−0.36

Additionally, the optimized geometries were employed to estimate the interaction energy of the selected dimers extracted from the crystal lattice. The computations were performed in the supermolecular approach within the CRYSTAL package at the DFT(B3LYP)/6-31G** level of theory, taking into account the basis-set superposition error (BSSE) and Grimme dispersion corrections (as implemented in the CRYSTAL code).

(c). *PIXEL Calculations.* For the purpose of CRYSTAL data verification, lattice energy were calculated in the OPiX package.¹⁷ The geometry were taken from the CRYSTAL optimization. The obtained structures were used to calculate the molecular electron density distribution by the means of standard quantum-chemical methods using the GAUSSIAN09 package at the MP2/6-31G** level of theory (with suggested default options). The electron density was then analyzed using the PIXEL module which allows for the calculation/estimation of dimer and lattice energies. In a crystal lattice stabilization energy computation a cluster of molecules within a radius of 20 Å was used.

■ ASSOCIATED CONTENT

● Supporting Information

Experimental details regarding synthesis, crystallographic data (residual density maps, geometrical parameters, CSD analysis), and computational details, supplementary results (atomic charges, scan parameters, geometries, energy considerations), and all crystallographic information files (CIFs). The CCDC numbers for the structures of fluorinated diboronic acids are fluoro-1,2-phenylenediboronic acid (mF) - 882252; 2,6-difluoro-1,4-benzenediboronic acid (26dF) - 882253; 2,5-difluoro-1,4-phenylenediboronic acid (25dF) - 882254; tetrafluoro-1,2-phenylenediboronic acid (tF) - 882255; 2,3-difluoro-1,4-phenylene-diboronic acid (23dF) - 882256. This material is available free of charge via the Internet at <http://pubs.acs.org>.

■ AUTHOR INFORMATION

Corresponding Author

*E-mail: kdurka@gmail.com (K.D.); kwozniak@chem.uw.edu.pl (K.W.).

Author Contributions

[§]Both authors contributed equally to this work.

Notes

The authors declare no competing financial interest.

■ ACKNOWLEDGMENTS

This work was supported by a grant from the National Science Centre (DEC-2011/01/N/ST5/05592). Authors would like to thank the Interdisciplinary Centre for Mathematical and Computational Modelling in Warsaw (G33-14) and the Wrocław Centre for Networking and Supercomputing for providing computational facilities. R.K. also thanks the Foundation for Polish Science for financial support within the "International Ph.D. Projects" programme. We gratefully acknowledge the Aldrich Chemical Co., Milwaukee, WI, USA, for a long-term collaboration.

■ REFERENCES

- (1) (a) Aakeröy, C. B.; Seddon, K. R. *Chem. Soc. Rev.* **1993**, 397–407. (b) Braga, D.; Grepioni, F.; Desiraju, G. R. *Chem. Rev.* **1998**, 98, 1375–1405. (c) Desiraju, G. R. *Angew. Chem., Int. Ed.* **1995**, 34, 2311–2327. (d) Desiraju, G. R. *Chem. Commun.* **1997**, 1475–1482. (e) Etter, M. C. *Acc. Chem. Res.* **1990**, 23, 120–126. (f) Prins, L. J.; Reinholdt, D. N.; Timmerman, P. *Angew. Chem., Int. Ed.* **2001**, 40, 2383–2426.
- (2) (a) Aakeröy, C. B.; Desper, J.; Levin, B. *CrystEngComm* **2005**, 7, 102–107. (b) Braga, D.; Polito, M.; Braccacini, M.; D'Addario, D.; Tagliavini, E.; Sturba, L. *Organometallics* **2003**, 22, 2142–2150.

- (c) Cyrański, M. K.; Jezierska, A.; Klimientowska, P.; Panek, J. J.; Sporzyński, A. *J. Phys. Org. Chem.* **2008**, *21*, 472–482. (d) Fournier, J.-H.; Maris, T.; Wuest, J. D.; Guo, W.; Galoppini, E. *J. Am. Chem. Soc.* **2003**, *125*, 1002–1006. (e) Norrild, J. C.; Sotofte, I. *J. Chem. Soc., Perkin Trans.* **2001**, *2*, 727–732. (f) Pilkington, M.; Wallis, J. D.; Larsen, S. *Chem. Commun.* **1995**, 1499–1500. (g) Shimpi, M. R.; Lekshmi, N. S.; Pedireddi, V. R. *Cryst. Growth Des.* **2007**, *10*, 1958–1963. (h) Maly, K. E.; Maris, T.; Wuest, J. D. *CrystEngComm* **2006**, *8*, 33–35. (i) Rodríguez-Cuamatzi, P.; Luna-García, R.; Torres-Huerta, A.; Bernal-Uruchurtu, M. I.; Barba, V.; Höpfl, H. *Cryst. Growth Design* **2009**, *9*, 1575–1583. (j) Pedireddi, V. R.; Lekshmi, N. S. *Tetrahedron Lett.* **2004**, No. 45, 1903–1905. (k) Rodríguez-Cuamatzi, P.; Arillo-Flores, O. I.; Bernal-Uruchurtu, M. I.; Höpfl, H. *Cryst. Growth Des.* **2005**, *5*, 167–175. (l) Rodríguez-Cuamatzi, P.; Vargas-Díaz, G.; Höpfl, H. *Angew. Chem., Int. Ed.* **2004**, *43*, 3041–3044. (m) Rodríguez-Cuamatzi, P.; Vargas-Díaz, G.; Maris, T.; Wuest, J. D.; Höpfl, H. *Acta Crystallogr.* **2004**, *E60*, o1316–o1318. (n) Varughese, S.; Sinha, S. B.; Desiraju, G. R. *Sci. China Chem.* **2011**, *54*, 1909–1919.
- (3) Hall, D. G. *Boronic Acids*; Wiley-VCH: Weinheim, Germany, 2005.
- (4) (a) Miyaura, N.; Suzuki, A. *Chem. Rev.* **1995**, *95*, 2457–2483. (b) Suzuki, A.; Diederich, F.; Stang, P. J. *Metal-Catalyzed Cross-Coupling Reactions*; Wiley-VCH: Weinheim, Germany, 1998.
- (5) (a) Soloway, A. H.; Tjarks, W.; Barnum, B. A.; Rong, R.-A.; Barth, R. F.; Codogni, I. M.; Wilson, J. G. *Chem. Rev.* **1998**, *98*, 1515–1562. (b) Yang, W.; Gao, X.; Wang, B. *Med. Res. Rev.* **2003**, *23*, 346–368.
- (6) (a) Lamère, J. F.; Lacroix, P.; Farfán, N.; Rivera, J. M.; Santillan, R.; Nakatani, K. *J. Mater. Chem.* **2006**, *16*, 1–9. (b) Li, Y.; Liu, Y.; Bu, W.; Guo, J.; Wang, Y. *Chem. Commun.* **2000**, 1551–1552.
- (7) (a) Furukawa, H.; Yaghi, O. M. *J. Am. Chem. Soc.* **2009**, *131*, 8875–8883. (b) Severin, K. *Dalton Trans.* **2009**, 5254–5264.
- (8) Allen, F. H. *Acta Crystallogr.* **2002**, *B58*, 380–388.
- (9) (a) Berger, R.; Resnati, G.; Metrangolo, P. *Chem. Soc. Rev.* **2011**, *40*, 3496–3508. (b) Chopra, D. *Cryst. Growth Des.* **2012**, *12*, 541–546. (c) Metrangolo, P.; Resnati, G. *Halogen Bonding: Fundamentals and Applications*; Springer: New York, 2008.
- (10) (a) Bertani, R.; Sgarbossa, P.; Venzo, A.; Lelj, F.; Amati, M.; Resnati, G.; Pilati, T.; Metrangolo, P.; Terraneo, G. *Coord. Chem. Rev.* **2010**, *254*, 677–695. (b) Reichenbacher, K.; Süß, H. J.; Stoeckli-Evans, H.; Bracco, S.; Sozzani, P.; Weber, E.; Hulliger, J. *New J. Chem.* **2004**, *28*, 393–397. (c) Thalladi, V. R.; Weiss, H.-C.; Bläser, D.; Boese, R.; Nangia, A.; Desiraju, G. R. *J. Am. Chem. Soc.* **1998**, *120*, 8702–8710.
- (11) Zimmer, L. E.; Sparr, C.; Gilmour, R. *Angew. Chem., Int. Ed.* **2011**, *50*, 11860–11871.
- (12) (a) Hernandez, M. Z.; Cavalcanti, S. M. T.; Moreira, D. R. *Curr. Drug Targets* **2010**, *11*, 303–314. (b) Jeschke, P. *Pest Manage. Sci.* **2010**, *66*, 10–27. (c) Tressaud, A. Haufe, G. *Fluorine and Health: Molecular Imaging, Biomedical Materials and Pharmaceuticals*; Elsevier: Amsterdam, 2008.
- (13) Durka, K.; Kurach, P.; Luliński, S.; Serwatowski, J. *Eur. J. Org. Chem.* **2009**, 4325–4332.
- (14) Allen, F. H.; Bruno, B. J. *Acta Crystallogr.* **2010**, *B66*, 380–386.
- (15) (a) Dovesi, R.; Orlando, R.; Civalieri, B.; Roetti, R.; Saunders, V. R.; Zicovich-Wilson, C. M. *Z. Kristallogr.* **2005**, *220*, 571–573. (b) Dovesi, R.; Saunders, V. R.; Roetti, R.; Orlando, R.; Zicovich-Wilson, C. M.; Pascale, F.; Civalieri, B.; Doll, K.; Harrison, N. M.; Bush, I. J.; D'Arco, P.; Llunell, M. *CRYSTAL09*; University of Torino: Torino, 2009.
- (16) Hoser, A.; Dominiak, P. M.; Wozniak, K. *Acta Crystallogr.* **2009**, *A65*, 300–311.
- (17) (a) Gavezzotti, A. *J. Phys. Chem. B* **2002**, *106*, 5145. (b) Gavezzotti, A. *J. Phys. Chem. B* **2003**, *107*, 2344–2353. (c) Gavezzotti, A. *CrystEngComm* **2003**, *5*, 429–438. (d) Gavezzotti, A. *J. Chem. Theor. Comput.* **2005**, *1*, 834–840.
- (18) Moller, C.; Plesset, M. S. *Pure Appl. Chem.* **1934**, *46*, 618–622.
- (19) Dunning, T. H. *J. Chem. Phys.* **1989**, *90*, 1007–1023.
- (20) (a) Spackman, M. A.; Byrom, P. G. *Chem. Phys. Lett.* **1997**, *267*, 215–220. (b) Wolff, S. K.; Grimwood, D. J.; McKinnon, J. J.; Jayatilaka, D.; Spackman, M. A. *CrystalExplorer, 2.1*; University of Western Australia: Perth, 2005–2007; (c) McKinnon, J. J.; Spackman, M. A.; Mitchell, A. S. *Acta Crystallogr.* **2004**, *B60*, 627–668. (d) Spackman, M. A.; Jayatilaka, D. *CrystEngComm* **2009**, *11*, 19–32.
- (21) Seethalekshmi, N.; Pedireddi, V. R. *Cryst. Growth Des.* **2007**, *5*, 944–949.
- (22) Larkin, J. D.; Bhat, K. L.; Markham, G. D.; Brooks, B. R.; Schaefer, H. F., III; Bock, C. W. *J. Phys. Chem. A* **2006**, *110*, 10633–10642.
- (23) Larkin, J. D.; Milkevitch, M.; Bhat, K. L.; Markham, G. D.; Brooks, B. R.; Bock, C. W. *J. Phys. Chem. A* **2008**, *112*, 125–133.
- (24) (a) Parkin, A.; Seaton, C. C.; Blagden, N.; Wilson, C. C. *Cryst. Growth Des.* **2007**, *7*, 531–534. (b) Thomas, L. H.; Blagden, N.; Gutmann, M. J.; Kallay, A. A.; Parkin, A.; Seaton, C. C.; Wilson, C. C. *Cryst. Growth Des.* **2010**, *10*, 2770–2774.
- (25) APEX2, Bruker AXS Inc.: Madison, WI, USA, 2010.
- (26) SAINT, 7.68A; Bruker AXS Inc.: Madison, WI, USA, 2010.
- (27) (a) Blessing, R. H. *J. Appl. Crystallogr.* **1989**, *22*, 396–397. (b) Blessing, R. H. *Acta Crystallogr.* **1995**, *A51*, 33–38.
- (28) *CrysAlis CCD/CrysAlis RED*, 171.33.66; Oxford Diffraction Ltd.: Abingdon, U.K., 2007.
- (29) Sheldrick, G. M. *Acta Crystallogr.* **2008**, *A64*, 112–122.
- (30) Frisch, M. J.; Trucks, G. W.; Schlegel, H. B.; Scuseria, G. E.; Robb, M. A.; Cheeseman, J. R.; J. A. Montgomery, J.; Vreven, T.; Kudin, K. N.; Burant, J. C.; Millam, J. M.; Iyengar, S. S.; Tomasi, J.; Barone, V.; Mennucci, B.; Cossi, M.; Scalmani, G.; Rega, N.; Petersson, G. A.; Nakatsuji, H.; Hada, M.; Ehara, M.; Toyota, K.; Fukuda, R.; Hasegawa, J.; Ishida, M.; Nakajima, T.; Honda, Y.; Kitao, O.; Nakai, H.; Klene, M.; Li, X.; Knox, J. E.; Hratchian, H. P.; Cross, J. B.; Bakken, V.; Adamo, C.; Jaramillo, J.; Gomperts, R.; Stratmann, R. E.; Yazyev, O.; Austin, A. J.; Cammi, R.; Pomelli, C.; Ochterski, J. W.; Ayala, P. Y.; Morokuma, K.; Voth, G. A.; Salvador, P.; Dannenberg, J. J.; Zakrzewski, V. G.; Dapprich, S.; Daniels, A. D.; Strain, M. C.; Farkas, O.; Malick, D. K.; Rabuck, A. D.; Raghavachari, K.; Foresman, J. B.; Ortiz, J. V.; Cui, Q.; Baboul, A. G.; Clifford, S.; Cioslowski, J.; Stefanov, B. B.; Liu, G.; Liashenko, A.; Piskorz, P.; Komaromi, I.; Martin, R. L.; Fox, D. J.; Keith, T.; Al-Laham, M. A.; Peng, C. Y.; Nanayakkara, A.; Challacombe, M.; Gill, P. M. W.; Johnson, B.; Chen, W.; Wong, M. W.; Gonzalez, C.; Pople, J. A. *Gaussian09*; Gaussian, Inc.: Wallingford, 2010.
- (31) Lee, C.; Yang, W.; Parr, R. G. *Phys. Rev. B* **1988**, *37*, 785–789.
- (32) Krishnan, R.; Binkley, J. S.; Seeger, R.; Pople, J. A. *J. Chem. Phys.* **1980**, *72*, 650–654.
- (33) (a) Grimme, S. *J. Comput. Chem.* **2004**, *25*, 1463–1473. (b) Grimme, S. *J. Comput. Chem.* **2006**, *27*, 1787–1799.